Gravity Wave Structure between 60 and 90 km Inferred from Space Shuttle Reentry Data

DAVID C. FRITTS

Geophysical Institute and Department of Physics, University of Alaska, Fairbanks, Alaska

ROBERT C. BLANCHARD

NASA Langley Research Center, Hampton, Virginia

LAWRENCE COY

Department of Earth and Atmospheric Sciences, St. Louis University, St. Louis, Missouri

(Manuscript received 2 March 1988, in final form 22 August 1988)

ABSTRACT

Density fluctuations obtained along seven space shuttle reentry tracks are used in this paper to examine the horizontal structure and the vertical distribution of density variance in the mesosphere and lower thermosphere. The tracks lie primarily over open ocean at middle and low latitudes and represent the only measurements of horizontal atmospheric structure at these heights available to date. The density fluctuations are interpreted in terms of gravity wave motions and reveal significant density (and velocity) variance at horizontal scales ranging from ~10 to 1000 km. Fluctuation amplitudes are used to infer corresponding velocity perturbations and characteristic vertical scales and frequencies of the wave spectrum. Results suggest that the mean velocity variance is smaller over the Pacific ocean than observed over major land masses and that the variance increases with height in a manner consistent with that expected in the presence of wave saturation processes.

1. Introduction

The recognition of the central role of gravity waves in the dynamics of the middle atmosphere has stimulated a number of studies of their characteristics and variability in this region. These studies have involved a variety of observational techniques and have attempted to identify the frequency and wavenumber composition of the wave spectrum, as well as its variability, in order to understand its middle atmosphere effects. Radar-derived frequency spectra compiled by Balsley and Carter (1982), Vincent (1984), and Balsley and Garello (1985) have revealed a mean frequency spectrum in the mesosphere and lower thermosphere that exhibits only slight amplitude variations and a slope near $-5/3$ while vertical wavenumber spectra suggest a saturated gravity wave spectrum (Dewan et al. 1984; Smith et al. 1987; Fritts and Chou 1987; Fritts et al. 1988a) with a high-wavenumber slope near -3.

Other studies have addressed the propagation, saturation, and characteristics of individual wave motions or examined gravity wave parameters, energies, momentum fluxes, and variability in a statistical manner. Radar and optical studies by Gavrilov and Shved (1982), Vincent and Reid (1983), Smith and Fritts (1983), Meek et al. (1985a), Reid (1986), Reid and Vincent (1987a), and Gardner and Voelz (1987) provided information on the periods, phase speeds (and directions), and horizontal and vertical scales of individual wave motions while Fritts et al. (1988b) used rocket and radar data to examine the conditions leading to wave field instability and turbulence generation. Gravity wave energies and their temporal variability were examined by Meek et al. (1985b) and Vincent and Fritts (1987) while Vincent and Reid (1983), Smith and Lyjak (1985), Fritts and Vincent (1987), and Reid and Vincent (1987b) provided radar or satellite-based estimates of the gravity wave momentum flux and divergence in the mesosphere and lower thermosphere.

Despite the importance of information on horizontal scales of gravity wave motions, however, our knowledge of this wave parameter relies more on inference than on direct measurements and is among the least quantified at present. Yet a detailed knowledge of the horizontal wavenumber spectrum and its geographic and temporal variability is essential if we are to understand the transports of energy and momentum by gravity wave throughout the middle atmosphere.

The purpose of this paper is to utilize a unique dataset to obtain information on the horizontal scales of gravity wave motions in the mesosphere and lower

Corresponding author address: Dr. David C. Fritts, Geophysical Institute and Department of Physics, University of Alaska, Fairbanks, AK 99775-0800.

thermosphere and on the corresponding wave amplitudes and inferred vertical scales and intrinsic frequencies. These data were obtained with high-resolution accelerometers aboard seven NASA space shuttles that provided information on atmospheric density between ~60 and 150 km altitudes during reentry from earth orbit. Our emphasis here will be on the data obtained below 90 km altitude, most of which represents essentially horizontal sections through the upper mesosphere. The data acquisition, processing, and flight track information are discussed in section 2. Presented in section 3 are the density fluctuations, horizontal wavenumber spectra, and inferred wave variances, scales, and frequencies. The results of our analysis are compared with previous studies in section 4, and our conclusions are presented in section 5.

2. Data acquisition and analysis

The atmospheric density profiles discussed in this paper were computed for each of seven reentries using data obtained with the Inertial Measurement Unit (IMU) used for onboard navigation and guidance on each space shuttle and the High Resolution Accelerometer Package (HIRAP) mounted aboard the shuttles *Challenger* and *Columbia*. These are three-axis accelerometers where the HIRAP provides a data rate of 174 Hz and an accuracy of 2–10 ($\times 10^{-6}$ g). Together with an estimate of the aerodynamic drag coefficient using pressure sensors aboard one shuttle and knowledge of the spacecraft velocity and area/mass ratio, these data permit a computation of the atmospheric density at each sample interval. The resulting density estimates were then averaged for 1 sec after removing those values obtained during thrust or other activity. The usable data extend from 60 to 160 km altitude, with the IMU contributing primarily at lower altitudes and the HIRAP at greater heights. The density estimates presented here are shown relative to the 1976 U.S. Standard Atmosphere. Additional information on the HIRAP experiment and the computation of atmospheric density is provided by Blanchard and Rutherford (1985) and Blanchard and Buck (1986).

Seasonal and flight track information for the reentries examined here is summarized in Table 1. The reentry tracks between 90 and 60 km altitudes are shown in Fig. 1. Figure 2 shows height versus horizontal position for reentry 24. Note that the data considered here are almost exclusively over open ocean, with each flight containing an ~4000 km near-horizontal segment between ~78 and 60 km.

TABLE 1. Reentry date and 90-km location for each of the space shuttle flights considered in this paper.

Reentry	Date	Lat. (90 km)	Long. (90 km)
6	9 Apr 1983	17°N	174°W
7	24 Jun 1983	27°N	181°W
8	5 Sep 1983	24°N	178°W
9	8 Dec 1983	56°N	198°W
11	11 Feb 1984	28°N	144°W
13	13 Apr 1984	16°N	177°W
24	6 May 1985	18°S	145°W

3. Data presentation

a. Density fluctuations and horizontal scales

The fractional density fluctuations, $\rho'/\bar{\rho}$, computed each second are shown for seven reentries (6, 7, 8, 9, 11, 13 and 24) along an ~4000 km horizontal track in Fig. 3. Here, ρ' and $\bar{\rho}$ are the perturbation and mean (1976 U.S. Standard Atmosphere) densities at each altitude, the mean and linear trend have been removed from each profile, and fluctuations have been scaled to the adjusted mean values. As noted previously the one second data represent a horizontal resolution of ~7 km near 80 km and ~5 km near 60 km altitude. Each reentry track was inclined ~0.3° below horizontal (a descent of 1 km in 200 km) at these heights in order to allow for gradual braking of the space shuttle.

Several features of the fractional density data are immediately obvious. First, there is considerable variability from one reentry to another in both fluctuation amplitudes and horizontal scales. Reentry 6 (Fig. 3, top), for example, exhibits a clear ~1000 km horizontal wavelength with $\rho'/\bar{\rho} \sim 0.01$–$0.02$, a high horizontal wavenumber component ($\lambda_s \sim$ 10–20 km, where λ_s is the wavelength along the reentry track) with $\rho'/\bar{\rho} \sim 0.01$, and very small fluctuation amplitudes at intermediate scales. The later reentries, in contrast, reveal much richer spectra of horizontal fluctuations with significant power at intermediate scales ($\rho'/\bar{\rho} \sim 0.01$–$0.05$ and $\lambda_s \sim$ 20–500 km). There is also considerable variability in the distribution of wave amplitudes and scales along the track, with reentries 6–9 exhibiting obvious decreases in wave amplitudes and scales in descending from 78 to 60 km and reentries 11, 13 and 24 exhibiting fairly uniform amplitudes throughout. Finally, while most of the density data are characterized by relatively slow variations in fluctuation amplitudes, there are several instances of strong, localized oscillations or apparent density jumps ($\rho'/\bar{\rho} \sim 0.03$–$0.05$) at horizontal scales of ~20–50 km. These are particularly prevalent in reentries 9, 11 and 13, but rapid density changes are also seen to occur in reentry 24. The oscillations are likely indications of localized, high-frequency wave activity whereas the apparent density jumps may result from wave superposition or possible nonhydrostatic wave phenomena.

We have assumed in the above discussion and in the data presentation in Fig. 3 that the density fluctuations are due to horizontal rather than vertical variations. This assumption will now be justified. First let us take $\rho'/\bar{\rho} \sim 0.01$ as a representative fluctuation amplitude. Using the linear thermodynamic equation

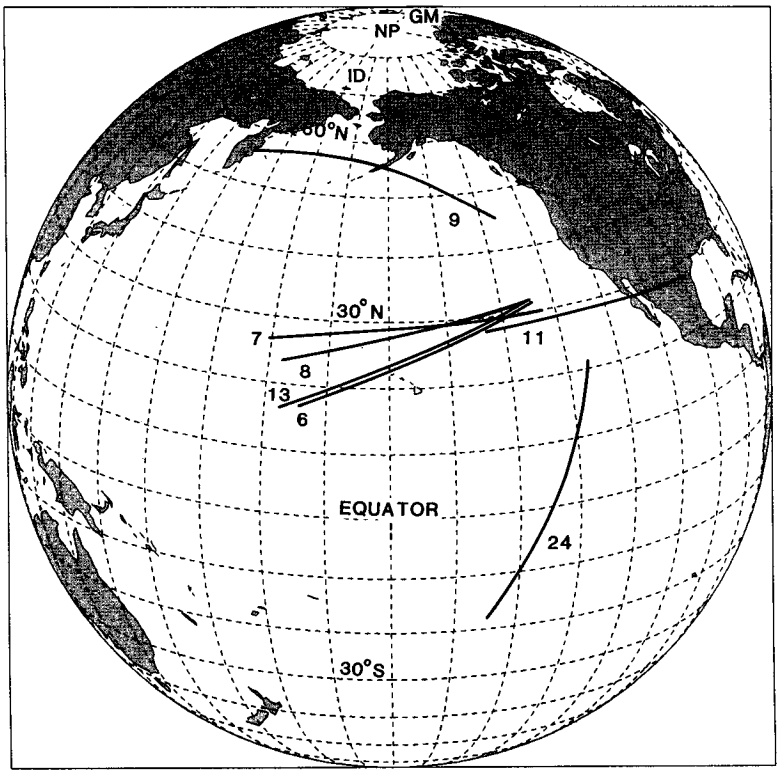

FIG. 1. Flight tracks between 90 and 60 km altitudes for the seven reentries included in this study. Note that, except for the lowest portion of reentry 11, all the density data were obtained over open ocean.

and the equation of state, the amplitude of the fractional density fluctuation for hydrostatic wave motions may be written

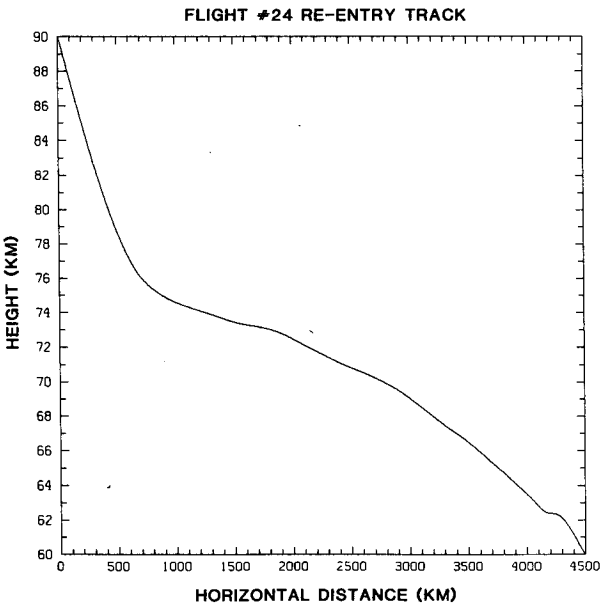

FIG. 2. Flight track for reentry 24 in the altitude range of interest. Above 75 km the descent rate is ~1:50. Below 75 km, it is ~1:200.

$$\frac{\rho'}{\bar{\rho}} = \frac{N^2 u'}{mg(c - \bar{u})} \tag{1}$$

where N is the Brunt–Väisälä frequency, m the vertical wavenumber, g the gravitational acceleration, and u' and $(c - \bar{u})$ the horizontal perturbation velocity and the intrinsic phase speed of the wave motion. Then using the dispersion relation for gravity waves with $N^2 \gg \omega^2$,

$$m^2 = \frac{k^2 N^2}{\omega^2 - f^2} = \frac{k^2 N^2}{\omega^2 \delta_-} \tag{2}$$

we obtain

$$\frac{\rho'}{\bar{\rho}} = \frac{N \delta_-^{1/2}}{g} u'. \tag{3}$$

With $N = 0.02$ rad s^{-1} and $\delta_- = (1 - f^2/\omega^2) \sim 1$, this implies a 5 m s^{-1} horizontal perturbation velocity for a density fluctuation of 0.01. For low-frequency motions, however, $\delta_- < 1$ and the implied wave velocities are larger. A total energy spectrum with a frequency dependence of the form $F(\omega) \sim \omega^{-p}$ has a ratio of kinetic to potential energy equal to p because of the influence of rotational effects at low frequencies (VanZandt 1985). As noted earlier, p appears to have a value near $\frac{5}{3}$ in the atmosphere (Balsley and Carter 1982).

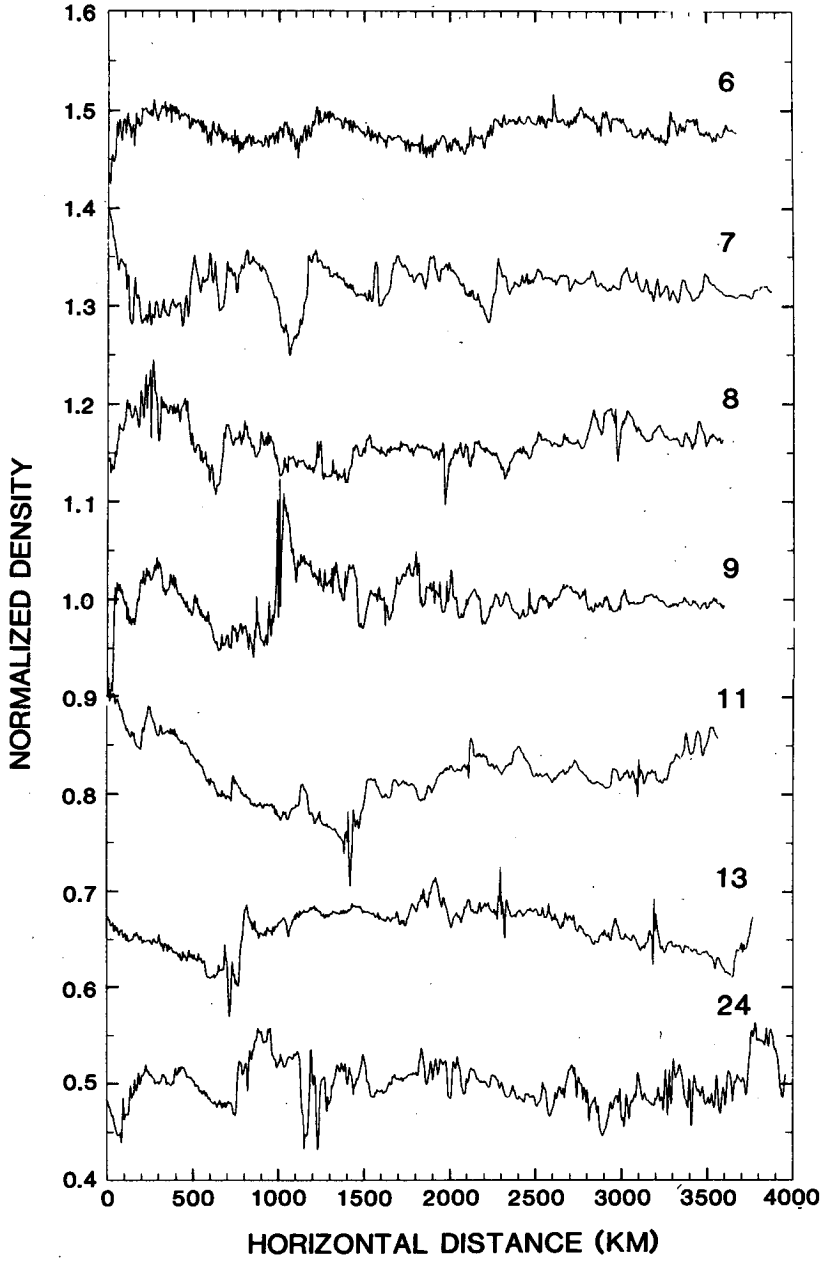

FIG. 3. Normalized densities (measured relative to the mean) versus horizontal position for each of the seven reentries between 78 and 60 km. Successive profiles are displaced from that for reentry 9 by 0.16 on the density scale. The data are at one second intervals and correspond to a horizontal resolution of ~6 km. Significant amplitudes are observed at scales ranging from ~20–1000 km.

We also know that saturation processes limit wave velocities to values near their intrinsic phase speeds (Fritts 1984) so that $u' \sim (c - \bar{u})$, suggesting that a density fluctuation of 0.01 must correspond to a minimum vertical wavelength

$$\lambda_z(\min) = \frac{2\pi}{m} \sim \frac{2\pi u'}{N} \sim 500\pi m. \qquad (4)$$

This is ~25 times larger, however, than the minimum vertical scale over which such fluctuations are seen, $\lambda_z \sim 12$ km/200 ~ 60 m, assuming fluctuations are due to vertical rather than horizontal variations in density. Thus the small-scale fluctuations can only be associated with primarily horizontal variations in atmospheric structure. Finally, we note that the descent angle is more gradual than the phase surface slopes, k/m

$\sim \omega\delta_-^{1/2}/N$, of all but the lowest-frequency motions, suggesting, in addition, that the reentry track may be regarded as horizontal for purposes of horizontal wavelength estimates.

In order to address the vertical distribution of wave variance later in this section, we present in Fig. 4 the vertical profiles of inferred density fluctuations for all seven reentries between 60 and 90 km, but recognize that the density fluctuations in most cases do not represent vertical wave structure. As noted earlier, there is a clear tendency in the first four reentries (6–9) for wave amplitudes and (horizontal) scales to increase with height up to ~80 km. When the height profiles are extended to 90 km, this tendency is observed in the later reentries as well. The growth in wave amplitudes is considerably more gradual than expected for conservative wave motions, however, and thus supports the view of a gradual spectral evolution consistent with wave saturation advanced by Smith et al. (1987). Vertical profiles of density variance will be presented and discussed in more detail later in this section. It should be noted here as an aside that the density estimates at heights above ~80 km were obtained with the same temporal resolution as those below, but that the vertical spacing is larger because the descent angle is larger above ~80 km (see Fig. 2). Thus, both provide reasonable estimates of wave amplitudes and, in particular, the lower data with higher apparent "vertical" resolution do not require vertical averaging for a valid comparison with the coarser vertical resolution data above.

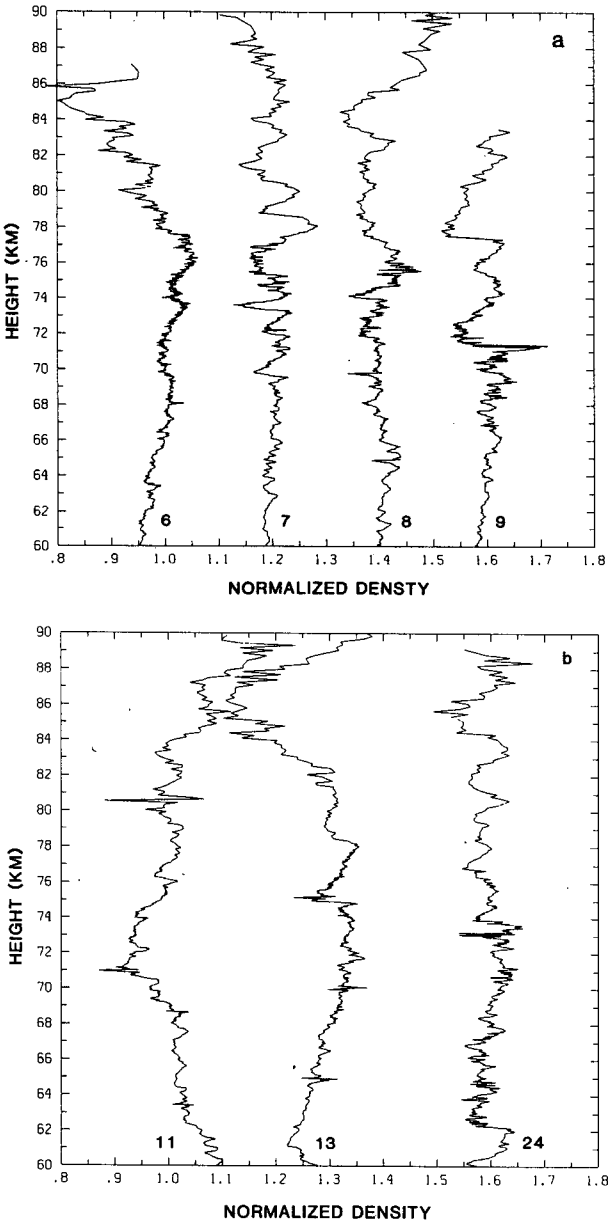

FIG. 4. Normalized densities between 60 and 90 km altitudes. Reentries 6–9 and 11, 13 and 24 are shown in (a) and (b), respectively. Successive profiles are displaced by 0.2 and 0.3 in (a) and (b). Note the tendency for amplitudes and scales to increase with height. The scales, however, are more representative of horizontal than of vertical wave structure because of the shallow descent angle.

b. *Fluctuation spectra*

We describe in this section the wavenumber spectra of the fractional density fluctuations obtained from the space shuttle accelerometer data. These spectra allow us to examine the distribution of wave variance with horizontal wavenumber along the track, $k_s = 2\pi/\lambda_s$, and to estimate the mean spectral characteristics of the motion field. Each spectrum was computed from density data at 556 points (a horizontal distance of ~3336 km) between 76 and 60 km after removal of a mean and linear trend from the data segment. A Hanning window was employed to avoid spurious effects of mismatched end points, and the resulting spectra were corrected for window effects. It should also be noted that the spectra were computed along slanted trajectories and that the wave variance was not uniform in height. Thus there is a potential for some spectral leakage as a result. Because the variance increase with height was small and the descent rate was much smaller than a typical gravity wave phase slope (~1:30), however, we anticipate the spectra presented here to be reasonably accurate estimates of horizontal wavenumber spectra.

The wavenumber spectra obtained for all of the reentries between ~76 and 60 km are shown in Fig. 5 and, like the fractional density data, suggest considerable variability between reentries in wave amplitudes and horizontal scales. That for reentry 6 exhibits the deficit of wave variance at intermediate scales noted in the discussion of Fig. 3 while later reentries are more consistent with the mean spectrum and contain more variance at intermediate scales.

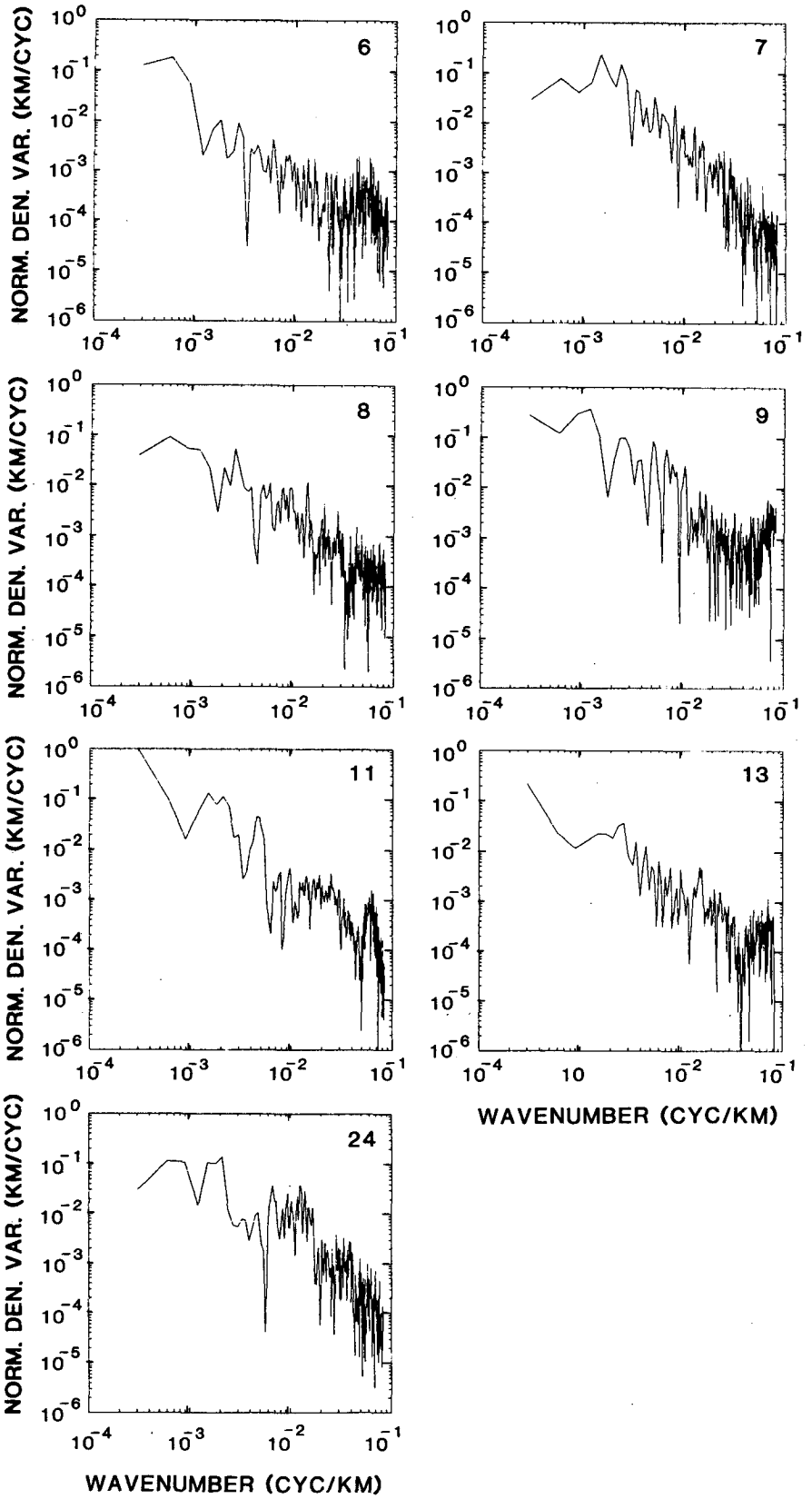

FIG. 5. Horizontal wavenumber spectra computed from 556 seconds (~3336 km) of data between ~76 and 60 km altitudes for the seven reentries. Note the significant differences in spectral amplitude and shape for the different flights.

The mean wavenumber spectrum of horizontal density variance shown in Fig. 6a reveals a distribution with a small negative slope at small wavenumbers and an increasingly negative slope as k_s increases, qualitatively consistent with horizontal wavenumber spectra at scales less than ~500 km obtained in the troposphere and lower stratosphere using GASP aircraft data by Nastrom and Gage (1985). In principle, this behavior should mirror the distribution of wave variance with vertical wavenumber observed in the lower and middle atmosphere using a variety of techniques (Dewan et al. 1984; Smith et al. 1987; Chanin and Hauchecorne 1987; Fritts et al. 1988a), but with a smaller characteristic wavenumber due to the tendency for horizontal scales to exceed vertical scales for most intrinsic frequencies, provided the wavenumber and frequency dependence of the gravity wave spectrum is approximately separable (VanZandt 1982, 1985).

The mean spectrum departs, however, from the -3 slope at high wavenumbers anticipated for a saturated spectrum of gravity waves (Dewan and Good 1986; Smith et al. 1987). There are at least two possible explanations for this. First, there is some evidence of a noise floor in the individual and mean spectra at high wavenumbers which could act to mask a steeper slope at $k_s > 10^{-2}$ cycles per kilometer (cpk). Subtracting this noise background would bring the slope for $k_s > 10^{-2}$ cpk near -3 and into agreement with observations of a saturated vertical wavenumber spectrum. Alternatively, a slope less than -3 may represent a departure from the separability observed at low frequencies, as noted by Fritts and Chou (1987) and Pinkel (1985) in the lower stratosphere and in the ocean. If real, the larger variances at high wavenumbers in the present data suggest higher intrinsic frequencies than are associated with the more energetic motions at lower wavenumbers and a more significant role in the transports of energy and momentum than expected for lower-frequency motions at the same horizontal scales.

c. *Characteristic wave scales and mean variance*

Before proceeding with our discussion of characteristic wave scales, we note here that the measured wavenumber k_s will be smaller than the horizontal wavenumber k of the wave motion in the direction of propagation if this is not along the reentry track. In this case $k_s = k\cos\theta$, where θ is the angle between the track and the direction of wave propagation. If we also assume an isotropic wave field, then waves of wavenumber k contribute to a mean track wavenumber

$$k_s = k/2^{1/2} \tag{5}$$

suggesting an effective horizontal wavelength

$$\lambda_h = \frac{2\pi}{k} = \frac{2\pi}{k_s 2^{1/2}} \sim \lambda_s/2^{1/2} \tag{6}$$

that is statistically smaller than observed along the track.

The mean "area-preserving" energy-content spectrum shown in Fig. 6b exhibits a broad variance peak about a horizontal wavenumber $k_s \sim 2 \times 10^{-3}$ cpk ($\lambda_s \sim 500$ km). This implies a characteristic horizontal wavenumber, using Eq. (6),

$$k_* \sim 2.8 \times 10^{-3} \text{ cpk} \quad (\lambda_{h*} \sim 350 \text{ km}). \tag{7}$$

It should be noted here that the spectral peak at $k_s \sim 3 \times 10^{-4}$ cpk is contributed primarily from reentry 11 (see Fig. 5) and is not representative of the other reentries.

We can likewise estimate the characteristic vertical scale and thus the characteristic intrinsic frequency of the motion spectrum provided we have a knowledge

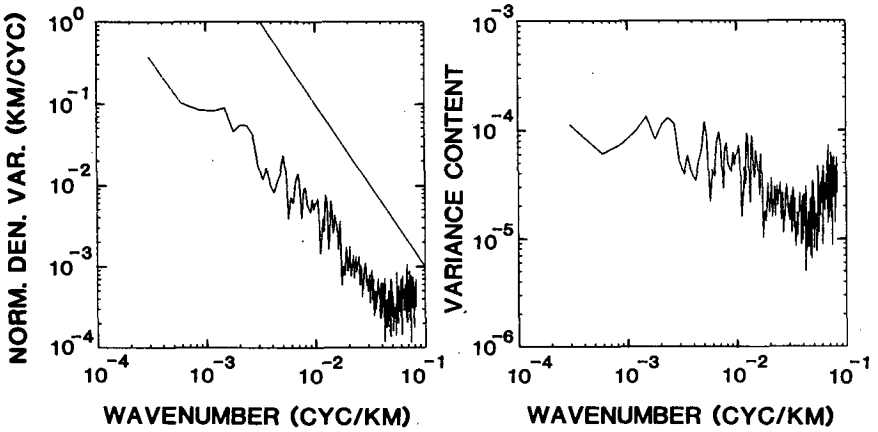

FIG. 6. Mean horizontal wavenumber spectrum for the seven reentries in (a) standard and (b) variance content form. A slope of -2 is shown for reference in (a). Note both the dominant horizontal scale, $\lambda_s \sim 500$ km, and the apparent noise floor for $k_s > 3 \times 10^{-2}$ cpk that may act to bias the spectrum away from a steeper slope at large k_s.

of the total wave variance. This can be obtained in two ways. Using Eq. (3), we can estimate the total horizontal velocity variance of the motion spectrum. From the fractional density profiles shown in Fig. 3, we infer an rms density fluctuation of $(\rho'/\bar{\rho})_{\rm rms} \sim 0.015$ between 60 and 76 km, corresponding to an rms horizontal velocity $u'_{\rm rms} \sim 7.5p^{1/2}$ m s^{-1} and a total horizontal velocity variance $\sim 60p$ m^2 s^{-2}. As noted earlier, the factor p obtains from the departure from energy equipartition due to rotational effects when the potential and kinetic energies are integrated over all frequencies. Alternatively, we can compute the average variance by integrating over the mean horizontal wavenumber spectrum. This yields a comparable value.

Now in order to infer the characteristic (mean) vertical scale and intrinsic frequency, we assume a saturated vertical wavenumber spectrum of the form

$$F_u(m) = \frac{N^2}{6m_*^3} \frac{\gamma}{1+\gamma^4}, \tag{8}$$

where $\gamma = m/m_*$, which is consistent both with observed wavenumber spectra for $m > m_*$ (Dewan et al. 1984; Smith et al. 1987; Fritts et al. 1988a) and with the requirement that the vertical wave action flux for $m < m_*$ be finite (VanZandt and Fritts 1988). Then equating the computed and inferred kinetic energies,

$$E = \frac{1}{2}\int_0^\infty F_u(m)dm = \frac{N^2}{12m_*^2}\int_0^\infty \frac{\gamma d\gamma}{1+\gamma^4} = \frac{\pi}{48}\frac{N^2}{m_*^2}, \tag{9}$$

we obtain

$$m_* = \frac{1}{4}\left[\frac{\pi}{3E}\right]^{1/2} N \sim 8.1 \times 10^{-2} \text{ cpk} \quad (\lambda_{z*} \sim 12 \text{ km}). \tag{10}$$

This is $\sim 28k_*$ and implies a characteristic intrinsic frequency

$$\omega_* \sim \frac{k_*}{m_*} N \sim 0.036N \sim 0.00071 \text{ rad s}^{-1}, \tag{11}$$

or a characteristic intrinsic period, $T_* \sim 2.4$ h, consistent with the mean frequency for a variance spectrum of the form ω^{-p} at a latitude of 25° and with the inferred dominance of low-frequency motions using radar techniques (Balsley and Carter 1982; Vincent 1984; Meek et al. 1985b; Balsley and Garello 1985; Vincent and Fritts 1987).

We also can estimate easily an approximate intrinsic frequency for individual wave motions from the observed density fluctuations and horizontal wavelengths. For wave motions with a vertical wavenumber spectrum described by Eq. (8), wave amplitudes are less than monochromatic saturation values due to wave superposition and the maximum amplitudes occur near the characteristic wavenumber m_*. From Eq. (8) with $\gamma = 1$ and a wavenumber bandwidth m_*, we obtain

$$\frac{u'^2}{2} \sim m_* F_u(l), \tag{12}$$

implying a vertical wavelength

$$\lambda_z = \frac{2\pi}{m_*} \sim \frac{15u'}{N} \sim \frac{15g}{N^2}\frac{\rho'}{\bar{\rho}}. \tag{13}$$

A wave motion with $\rho'/\bar{\rho} \sim 0.02$ and $\lambda_s \sim 50$ km yields $\omega/N \sim \lambda_z/\lambda_h \sim 0.2$, suggesting that waves with smaller amplitudes and/or larger horizontal wavelengths are likely to be hydrostatic, as assumed earlier. Thus, motions with $\rho'/\bar{\rho} \sim 0.02$ and $\lambda_s \sim 100$–500 km, as seen in a number of the fractional density profiles in Fig. 3, correspond to intrinsic wave periods $T_i \sim 1$–5 hr while the $\lambda_s \sim 1000$ km motion with $\rho'/\bar{\rho} \sim 0.015$ in Fig. 3 (top) suggests an intrinsic period $T_i \sim 10$ h. Small-scale, large-amplitude motions, however, do not satisfy the hydrostatic approximation and likely represent either ducted wave activity or components of the wave spectrum that propagate vertically very rapidly.

d. Vertical profiles of fractional density variance

The vertical profiles of fractional densities shown in Fig. 4 were used to compute estimates of the density variance in 5- and 10-km height intervals between 60 and 90 km altitude. The variance was computed for each interval after removal of a mean and linear trend and compensating the ratio $\rho'/\bar{\rho}$ for departures of $\bar{\rho}$ from the assumed mean density. This latter correction was applied because wave amplitudes are proportional to density perturbations relative to the local mean density. The resulting individual and mean variance profiles are shown in Figs. 7 and 8 for the 5- and 10-km intervals.

There is a clear tendency for most of the individual profiles to exhibit an increase of variance with height. This trend is also evident in the mean profiles. There are, nevertheless, variance minima in the individual profiles at various heights. We believe, however, that these minima are more likely indicative of horizontal than vertical variability of the wave spectrum, reflecting variable source or filtering conditions at lower levels of the atmosphere.

The mean fractional density variance inferred in 5-km intervals increases from 1.3×10^{-4} below 70 km to 1.3×10^{-3} between 85 and 90 km, revealing an increase by 10 in the potential energy (per unit mass) of the wave spectrum in this height interval. Using Eq. (3) with $\delta_- \sim p^{-1} = 3/5$ yields a corresponding velocity variance that increases from ~ 55 to 415 m^2 s^{-2}. Assuming a variation of energy with height of the form

$$E(z) \sim e^{z/H}E, \tag{14}$$

we obtain $H_E \sim 12$ km, implying a growth of wave energy with height that is substantially smaller than expected in the absence of wave dissipation and slightly

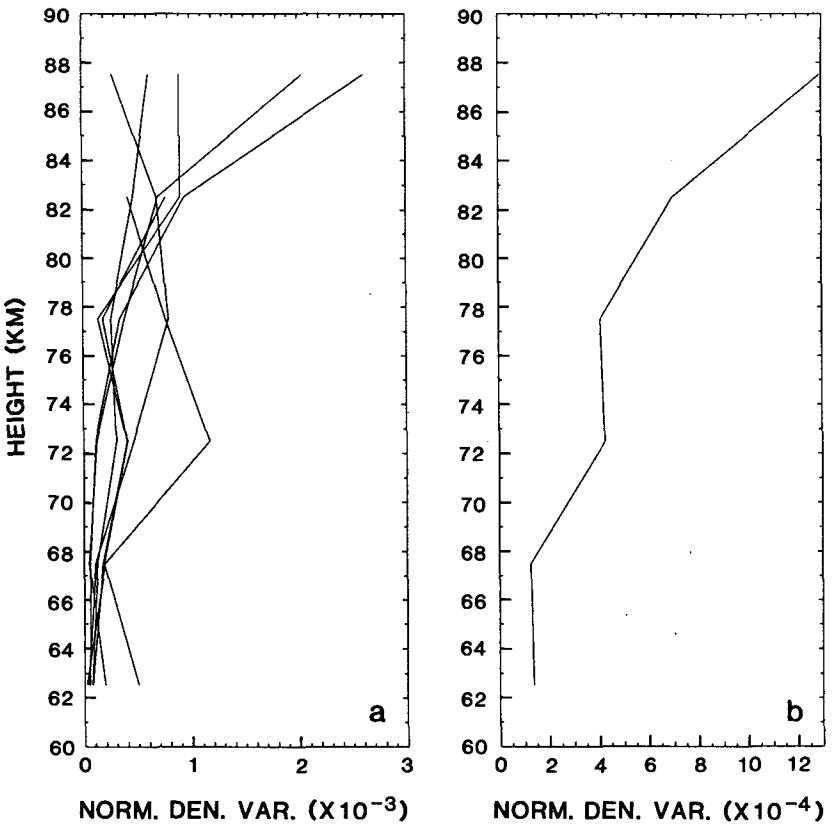

FIG. 7. Individual (a) and mean (b) normalized density variance profiles computed in 5-km height intervals. The mean profile exhibits an increase of 10 between 62.5 and 87.5 km, implying a scale height for wave energy growth of $H_E \sim 12$ km.

more rapid that estimated at lower levels of the atmosphere (Smith et al. 1987).

Below 75 km, the 5-km estimates of fractional density variance correspond to ~1000-km horizontal segments and thus include the majority of the variance in the individual spectra. Above 75 km, however, each 5-km variance estimate corresponds to a horizontal segment only ~250 km in length and so does not include the variance due to large-scale wave motions. Inspection of the vertical profiles (Fig. 4) suggests that this is not a large error for several of the reentries, but may be significant for others. For comparison, the variances computed in 10-km segments are shown in Fig. 8. Here, the mean increases from 1.7×10^{-4} at 65 km to 2.8×10^{-3} at 85 km, suggesting a more rapid variance growth with height with an e-folding scale $H_E \sim 7$ km. However, we consider this variance estimate to be too large for several reasons. First, an exponential growth height of 7 km implies approximate conservation of wave energy, in contrast to the saturation hypothesis and to other observations of larger H_E throughout the atmosphere. Second, variance at larger vertical scales may occur as a result of departures of the mean atmospheric structure from the assumed standard. Finally, particularly at greater heights and larger vertical scales, there may be significant variance due to tidal motions which we wish to exclude from our estimate of the variance due to gravity wave motions. Thus, we view the 5-km variance estimates as more representative of gravity wave amplitudes, but recognize that this may be somewhat of an underestimate at upper levels.

4. Comparison with other observations

It was shown in the previous section that rms fractional density fluctuations and horizontal wave velocities inferred during space shuttle reentries are generally ~0.01–0.05 and $5p^{1/2}$–$25p^{1/2}$ m s^{-1}, respectively, between 60 and 90 km altitude, implying a horizontal velocity variance of the wave spectrum of ~55–415 m^2 s^{-2} at these heights. Wave amplitudes and variances, however, appear to be significantly less than observed over land using radar and rocket techniques. The frequency spectra presented by Balsley and Carter (1982) and Balsley and Garello (1985), for example, reveal velocity variances at ~85 km of ~650–1300 m^2 s^{-2}, while Balsley et al. (1983), Vincent (1984), Meek et al. (1985b), and Vincent and Fritts (1987) presented evidence of variances for the entire gravity wave spectrum of ~1000 m^2 s^{-2} at these heights. These

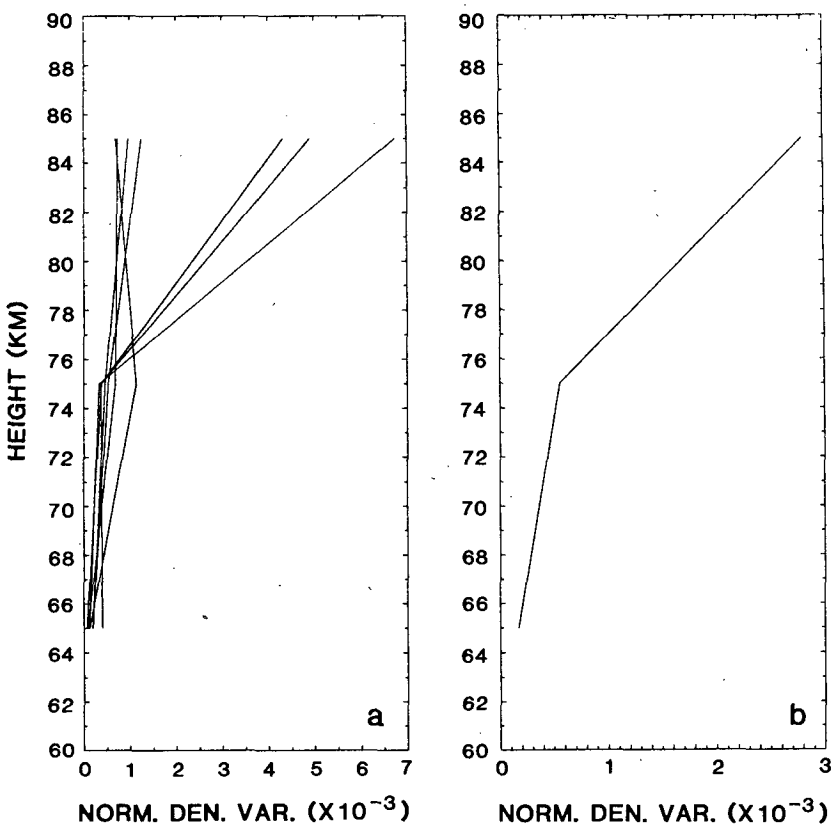

FIG. 8. As in Fig. 7, but for 10-km intervals. The implied growth with height in this case, however, allows for no dissipation of wave energy and may thus be an overestimate at upper levels.

values are approximately twice the variance inferred from the space shuttle data and are consistent with the findings of Nastrom et al. (1987) of enhanced velocity variances over major topography relative to plains and open ocean using GASP aircraft data in the troposphere and lower stratosphere. Together these observations reveal a less energetic motion spectrum over the oceans throughout the atmosphere and imply a major role of topography, and other sources enhanced over land, in the excitation of atmospheric gravity wave motions.

Our spectral observations also provide the first estimate of the characteristic horizontal wavenumber of the wave spectrum in the middle atmosphere, $k_* \sim 2.8 \times 10^{-3}$ cpk, or $\lambda_{h*} \sim 350$ km. Numerous other authors have reported horizontal wavelength estimates using radar and optical techniques (see Fritts 1984; Reid 1986). However, it has not been possible until now to obtain statistical information on the amplitudes and horizontal structure of atmospheric motions at mesospheric heights. This characteristic horizontal scale is ~3 times larger than that inferred from the GASP data of Nastrom and Gage (1985), recognizing that with a wavenumber spectrum of the form of Eq. (8) the characteristic scale (along the flight track) occurs at the wavenumber at which the spectrum has a slope of -1.

Assuming a saturated gravity wave spectrum, we also inferred a characteristic vertical scale of $\lambda_{z*} \sim 12$ km, somewhat smaller than that observed using radar and rocket data over land (Smith et al. 1987), due to the smaller wave energies inferred over the oceans. As noted by Nastrom et al. (1987), this implies a smaller role of the gravity wave spectrum over the oceans in the transports of energy and momentum relative to that over land.

Finally, we note that the observed growth of wave energy between 60 and 90 km heights, with an *e*-folding scale of $H_E \sim 12$ km, corresponds closely to that inferred throughout the atmosphere from the spectral energy densities observed near the tropopause and the mesopause using radar techniques (Balsley and Carter 1982; Balsley and Garello 1985). This is likely a result of the saturation of gravity wave motions at small vertical scales and of the consequent growth of wave amplitudes only at large (as yet unsaturated) vertical scales (Smith et al. 1987).

5. Conclusions

Atmospheric density data obtained from space shuttleborne accelerometers during seven reentries were used in this study to infer the characteristic scales and velocity variance of the gravity wave spectrum between 60 and 90 km altitude. The reentries were primarily at low latitudes over the central Pacific and were distributed throughout the year. The exceptions were reentries at 57°N and 35°S (9 and 24). Considerable variability was observed in the wave spectrum from one reentry to another and within individual profiles, presumably reflecting the inherent variability of source and filtering conditions in the underlying atmosphere. Horizontal wavelengths ranged from ~10–1000 km and horizontal velocity variances were ~55–415 $m^2 s^{-2}$ between 60 and 90 km. The presence of density fluctuations with large amplitudes and small horizontal scales are indicative of relatively high-frequency ($T < 1$ h) gravity waves, suggesting sources of such motions, perhaps convection and/or wind shear, at lower heights. As noted in other studies, however, the more energetic part of the motion spectrum occurs at lower frequencies, with $\lambda_h \gg \lambda_z$ and a characteristic intrinsic wave period of $T_* \sim 2.4$ h.

Inferred wave amplitudes and variances in the mesosphere were typically lower than observed over land at comparable heights using other techniques, suggesting both smaller characteristic vertical scales of the motion spectrum and smaller vertical fluxes of energy and momentum over the ocean. The observed growth of the velocity variance with height, however, was found to be consistent with that inferred from radar data obtained from heights near the tropopause and mesopause.

In summary, our results suggest that the gravity wave spectrum in the mesosphere over the ocean has many of the same characteristics observed over land, but is less energetic because of a different complement of lower atmospheric sources. This implies quantitatively different effects of gravity waves in the mesosphere and lower thermosphere over land and oceans and suggests a possible forcing of planetary-scale motions in response. These results are superficial at best, however, and should serve as an additional motivation for more comprehensive studies using ground-based techniques currently planned for several central Pacific sites.

Acknowledgments. The authors wish to thank Li Yuan for his assistance in preparing the figures. Support for DCF was provided by the SDIO/IST and managed by the Office of Naval Research under Contract N00014-86-K-0661. Support for LC at the University of Alaska was provided by the Division of Atmospheric Sciences of the National Science Foundation under Grant ATM-8404017.

REFERENCES

Balsley, B. B., and D. A. Carter, 1982: The spectrum of atmospheric velocity fluctuations at 8 and 86 km. *Geophys. Res. Lett.*, **9**, 465–468.

——, and R. Garello, 1985: The kinetic energy density in the troposphere, stratosphere and mesosphere: A preliminary study using the Poker Flat radar in Alaska. *Radio Sci.*, **20**, 1355–1362.

——, W. L. Ecklund and D. C. Fritts, 1983: VHF echoes from the high-latitude mesosphere and lower thermosphere: Observations and interpretations. *J. Atmos. Sci.*, **40**, 2451–2466.

Blanchard, R. C., and J. F. Rutherford, 1985: Shuttle orbiter high resolution accelerometer package experiment: Preliminary flight results. *J. Spacecr. Rockets*, **22**, 474–480.

——, and G. M. Buck, 1986: Rarefied-flow aerodynamics and thermosphere structure from shuttle flight measurements. *J. Spacecr. Rockets*, **23**, 18–24.

Chanin, M. L., and A. Hauchecorne, 1987: Lidar sounding of the structure and dynamics of the middle atmosphere. A review of recent results relevant to transport processes, *Transport Processes in the Middle Atmosphere*. NATO Advanced Studies Workshop, G. Visconti and R. Garcia, Eds., 459–477.

Dewan, E. M., and R. E. Good, 1986: Saturation and the "universal" spectrum for vertical profiles of horizontal scalar winds in the atmosphere. *J. Geophys. Res.*, **91**, 2742–2748.

——, N. Grossbard, A. F. Quesada and R. E. Good, 1984: Spectral analysis of 10 m resolution scalar velocity profiles in the stratosphere. *Geophys. Res. Lett.*, **11**, 80–83, Correction to "Spectral analysis of . . .", *Geophys. Res. Lett.*, **11**, 624.

Fritts, D. C., 1984: Gravity wave saturation in the middle atmosphere: A review of theory and observations. *Rev. Geophys. Space Phys.*, **22**, 275–308.

——, and H. G. Chou, 1987: An investigation of the vertical wavenumber and frequency spectra of gravity wave motions in the lower stratosphere. *J. Atmos. Sci.*, **44**, 3610–3624.

——, and R. A. Vincent, 1987: Mesospheric momentum flux studies at Adelaide, Australia: Observations and a gravity wave-tidal interaction model. *J. Atmos. Sci.*, **44**, 605–619.

——, T. Tsuda, T. Sato, S. Fukao and S. Kato, 1988a: Observational evidence of a saturated gravity wave spectrum in the troposphere and lower stratosphere. *J. Atmos. Sci.*, **45**, 1741–1759.

——, S. A. Smith, B. B. Balsley and C. R. Philbrick, 1988b: Evidence of gravity wave saturation and local turbulence production in the summer mesosphere and lower thermosphere during the STATE experiment. *J. Geophys. Res.*, **93**, 7015–7025.

Gardner, C. S., and D. G. Voelz, 1987: Lidar studies of the nighttime Sodium layer over Urbana, Illinois, 2, gravity waves. *J. Geophys. Res.*, **92**, 4673–4694.

Gavrilov, N. M., and G. M. Shved, 1982: Study of internal gravity waves in the lower thermosphere from observations of the nocturnal sky Airglow [OI] 5577A in Ashkhabad. *Ann. Geofis.*, **38**, 789–803.

Meek, C. E., I. M. Reid and A. H. Manson, 1985a: Observations of mesospheric wind velocities. I. Gravity wave horizontal scales and phase velocities determined from spaced wind observations. *Radio Sci.*, **20**, 1383–1402.

——, —— and ——, 1985b: Observations of mesospheric wind velocities. II. Cross sections of power spectral density for 48-8h, 8-1h, 1h-10 min over 60–110 km for 1981. *Radio Sci.*, **20**, 1383–1402.

Nastrom, G. D., and K. S. Gage, 1985: A climatology of aircraft wavenumber spectra observed by commercial aircraft. *J. Atmos. Sci.*, **42**, 950–960.

——, D. C. Fritts and K. S. Gage, 1987: An investigation of terrain effects on the mesoscale spectrum of atmospheric motions. *J. Atmos. Sci.*, **44**, 3087–3096.

Pinkel, R., 1985: A wavenumber-frequency spectrum of upper-ocean shear. *J. Phys. Oceanogr.*, **15**, 1453–1469.

Reid, I. M., 1986: Gravity wave motions in the upper middle at-

mosphere (60–110 km). *J. Atmos. Terres. Phys.*, **48,** 1057–1072.

——, and R. A. Vincent, 1987a: Measurements of the horizontal scales and phase velocities of short period mesospheric gravity waves at Adelaide, Australia. *J. Atmos. Terr. Phys.*, **49,** 1033–1048.

——, and R. A. Vincent, 1987b: Measurements of mesospheric gravity wave momentum fluxes and mean flow accelerations at Adelaide, Australia. *J. Atmos. Terr. Phys.*, **49,** 443–460.

Smith, A. K., and L. V. Lyjak, 1985: An observational estimate of gravity wave drag from the momentum balance in the middle atmosphere. *J. Geophys. Res.*, **90,** 2233–2241.

Smith, S. A., and D. C. Fritts, 1983: Estimations of gravity wave motions, momentum fluxes and induced mean flow accelerations in the winter mesosphere over Poker Flat, Alaska. *Proc. 21st Conference on Radar Meteorology,* Edmonton, 104–110.

——, D. C. Fritts and T. E. VanZandt, 1987: Evidence of a saturation spectrum of atmospheric gravity waves. *J. Atmos. Sci.*, **44,** 1404–1410.

VanZandt, T. E., 1982: A universal spectrum of buoyancy waves in the atmosphere. *Geophys. Res. Lett.*, **9,** 575–578.

——, 1985: A model for gravity wave spectra observed by Doppler sounding systems. *Radio Sci.*, **20,** 1323–1330.

——, and D. C. Fritts, 1988: A theory of enhanced saturation of the gravity wave spectrum due to increases in atmospheric stability. *Pure Appl. Geophys.*, in press.

Vincent, R. A., 1984: Gravity wave motions in the mesosphere. *J. Atmos. Terr. Phys.*, **46,** 119–128.

——, and I. M. Reid, 1983: HF Doppler measurements of mesospheric momentum fluxes. *J. Atmos. Sci.*, **40,** 1321–1333.

——, and D. C. Fritts, 1987: A morphology of gravity waves in the mesosphere and lower thermosphere over Adelaide, Australia. *J. Atmos. Sci.*, **44,** 748–760.